Doping Implications of Li Solid State Electrolyte $Li_7La_3Zr_2O_{12}$

Supporting Information

Kristoffer Eggestad,[1] Sverre M. Selbach,[1] and Benjamin A. D. Williamson[1]

[1] *Department of Materials Science and Engineering,*
NTNU Norwegian University of Science and Technology, Trondheim, Norway

Table S1 displays calculated lattice parameters of the tetragonal LLZO structure. The lattice parameters are obtained through hybrid density functional theory (DFT) calculations using the HSE06 functional[1]. Optimised atomic positions are displayed in Table S2.

Table S1: DFT optimised lattice parameters using HSE06 for the conventional tetragonal $Li_7La_3Zr_2O_{12}$ structure.

a, b	13.0851 Å
c	12.5530 Å
α, β, γ	90°

Table S2: DFT optimized atomic positions using HSE06 for the conventional $Li_7La_3Zr_2O_{12}$ structure.

Specie	a	b	c	Wyckoff
Li	1	0.75	0.125	8a
Li	0.821048	0.571048	-0.125	16f
Li	0.418562	0.414024	0.055851	32g
La	1	0.75	-0.125	8b
La	0.872077	1	0	16e
Zr	0.5	0.5	0.25	16c
O	0.534939	0.444969	0.403359	32g
O	0.945609	1.14675	0.284525	32g
O	0.850057	0.97249	0.196877	32g

The calculated dielectric tensor, used for the image charge correction, is displayed for the conventional unit cell in equation 1. It was estimated from the static dielectric tensor calculated using density functional perturbation theory (DFPT) performed with PBEsol and the high frequency dielectric tensor calculated with HSE06.

$$\varepsilon = \begin{pmatrix} 21.545 & 0 & \\ 0 & 21.545 & 0 \\ 0 & 0 & 32.939 \end{pmatrix} \tag{1}$$

Figure S1 displays the cubic LLZO structure with its Li sites. A Li site with Wyckoff label 48g is also often described, but this site is just the average position of the two 96h sites displayed in (b). Both Li sites are partially occupied and the 96h sites displayed in (b) cannot be occupied at the same time.

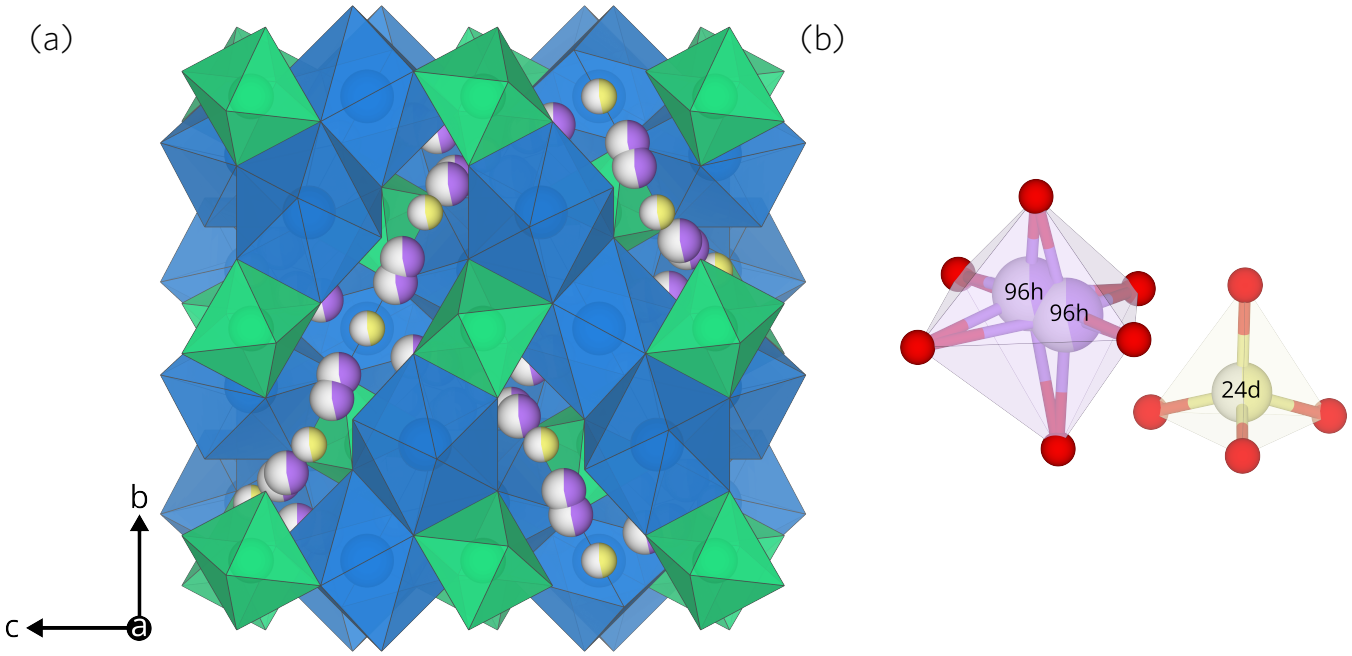

Figure S1: (a) The cubic LLZO structure. O ions are omitted for clarity. (b) Li sites. 96h in purple and 24d in yellow. Both Li sites are partially occupied. The grey parts of the atoms indicate partial occupancy and the figure is made using the visualisation software VESTA[2].

The stability region of tetragonal LLZO is displayed in Figure S2. The red dots show the chemical potentials used for the thermodynamic transition levels discussed in the main text. This set of chemical potentials corresponds to the chemical potential of oxygen in air at 1200°C.

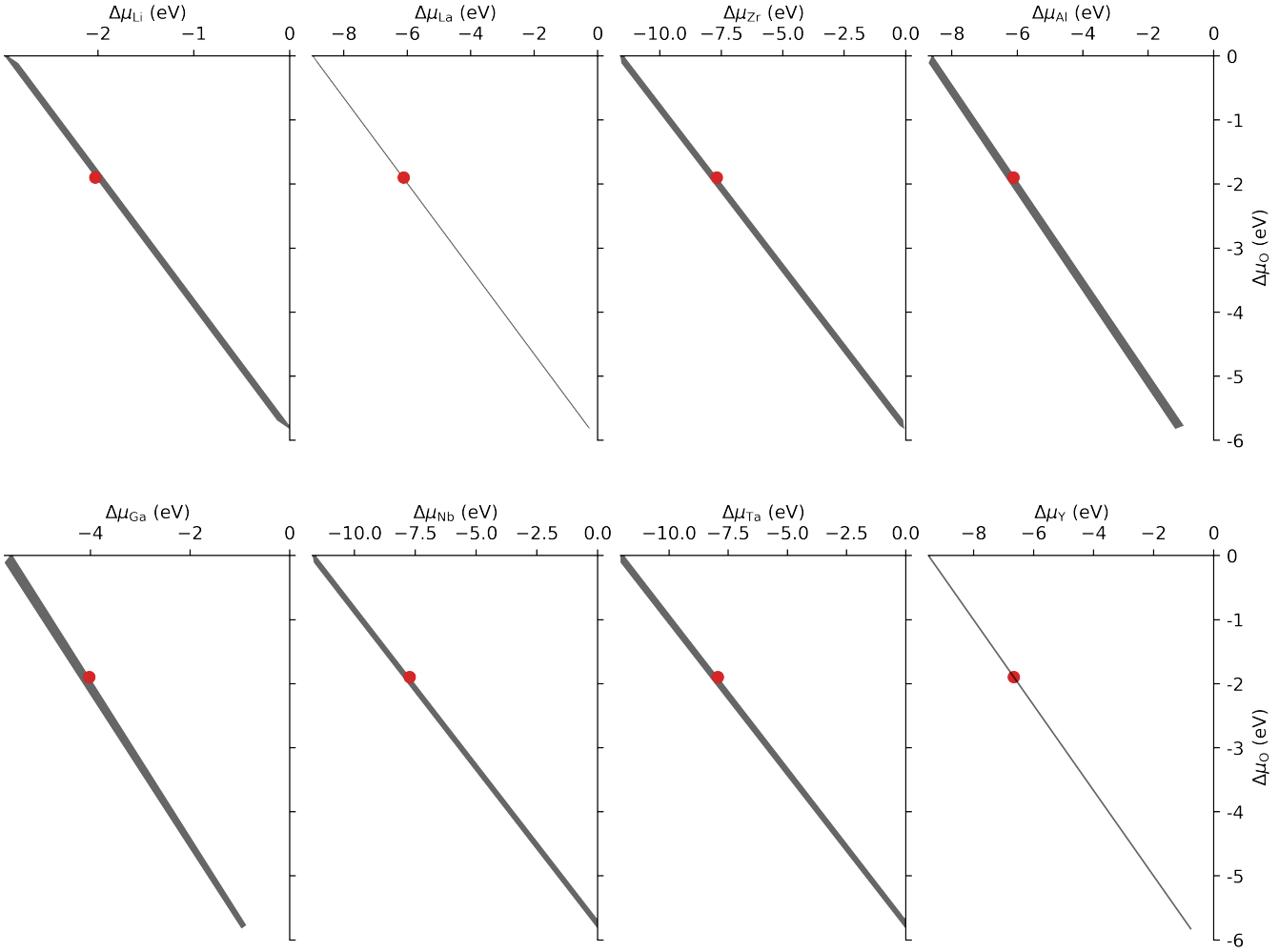

Figure S2: The calculated stability region for tetragonal $Li_7La_3Zr_2O_{12}$. The red circle indicates the chemical potential of O in air at 1200°C and the corresponding chemical potentials for the other elements.

The Li Frenkel defect, equation 2, is one of the most prominent defects in pristine LLZO. Equation 3, 4, 5 and 6 show the equations describing the response of dopants discussed in the main text.

$$\mathrm{Li}_{\mathrm{Li}}^{\mathrm{x}} + \mathrm{V}_{i}^{\mathrm{x}} \rightarrow \mathrm{V}_{\mathrm{Li}}^{\prime} + \mathrm{Li}_{i}^{\bullet} \tag{2}$$

$$(\mathrm{Al/Ga})_2\mathrm{O}_3 + 6\,\mathrm{Li}_{\mathrm{Li}}^{\mathrm{x}} \longrightarrow 2\,(\mathrm{Al/Ga})_{\mathrm{Li}}^{\bullet\bullet} + 4\,\mathrm{V}_{\mathrm{Li}}^{\prime} + 3\,\mathrm{Li}_2\mathrm{O} \tag{3}$$

$$(\mathrm{Nb/Ta})_2\mathrm{O}_5 + 2\,\mathrm{Zr}_{\mathrm{Zr}}^{\mathrm{x}} + 2\,\mathrm{Li}_{\mathrm{Li}}^{\mathrm{x}} \longrightarrow 2\,(\mathrm{Nb/Ta})_{\mathrm{Zr}}^{\bullet} + 2\,\mathrm{V}_{\mathrm{Li}}^{\prime} + \mathrm{Li}_2\mathrm{O} + 2\,\mathrm{ZrO}_2 \tag{4}$$

$$\mathrm{Y}_2\mathrm{O}_3 + 2\,\mathrm{La}_{\mathrm{La}}^{\mathrm{x}} \longrightarrow 2\,\mathrm{Y}_{\mathrm{La}}^{\mathrm{x}} + \mathrm{La}_2\mathrm{O}_3 \tag{5}$$

$$\mathrm{Y}_2\mathrm{O}_3 + 2\,\mathrm{Zr}_{\mathrm{Zr}}^{\mathrm{x}} + 2\,\mathrm{Li}_2\mathrm{O} + 2\,\mathrm{V}_{i}^{\mathrm{x}} \longrightarrow 2\,\mathrm{Y}_{\mathrm{Zr}}^{\prime} + 2\,\mathrm{Li}_{i}^{\bullet} + 2\,\mathrm{ZrO}_2 \tag{6}$$

The unit cell of tetragonal LLZO has two non-equivalent Li paths. A path including all Li Wyckoff sites is displayed in the main text in Figure 1, while the other alternative path is displayed in Figure S3.

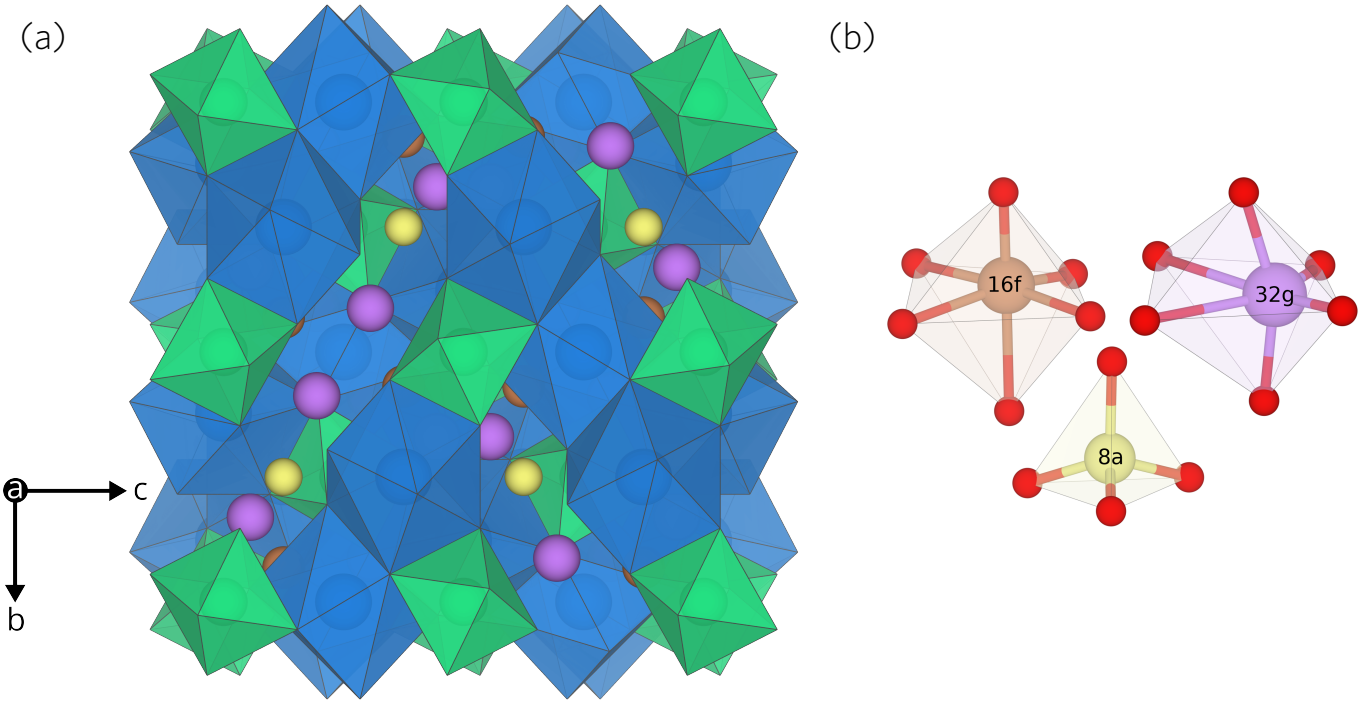

Figure S3: (a) The tetragonal LLZO structure with the three different Li sites (b). Here another Li path is displayed where the 16f sites are not used, but with slightly longer jumps.The figure is made using the visualisation software VESTA[2].

The following 6 tables, Table S3, S4, S5, S6, S7 and S8, displays calculated energies of formation per atom, using the PBEsol functional[3], of competing phases to the pristine and the doped LLZO structure.

Table S3: Energy of formation per atom and **k** points for competing phases to LLZO from DFT calculations with PBEsol.

Phases	Energy/atom (eV)	**k** points (Γ-centred)
La_2O_3	-3.85	$3 \times 3 \times 3$
$La_2Zr_2O_7$	-3.97	$4 \times 4 \times 4$
Li_2O	-2.08	$8 \times 8 \times 8$
Li_2O_2	-1.77	$8 \times 8 \times 3$
Li_2ZrO_3	-3.11	$5 \times 5 \times 4$
$Li_6Zr_2O_7$	-2.92	$4 \times 4 \times 2$
Li_8ZrO_6	-2.5	$5 \times 5 \times 5$
LiO_8	-0.88	$5 \times 5 \times 5$
Zr_3O	-1.63	$5 \times 5 \times 5$
Zr_4O	-1.31	$5 \times 5 \times 5$
ZrO_2	-3.94	$4 \times 4 \times 4$

Table S4: Energy of formation per atom and **k** points for competing phases including Al calculated using the PBEsol functional.

Phases	Energy/atom (eV)	**k** points (Γ-centred)
Al_2O_3	-3.48	$6 \times 6 \times 6$
La_3Al_{11}	-0.39	$3 \times 5 \times 5$
La_3AlO	-1.5	$4 \times 4 \times 4$
$La_4Al_2O_9$	-3.77	$3 \times 2 \times 2$
LaAl	-0.41	$14 \times 14 \times 14$
$LaAl_2$	-0.5	$15 \times 15 \times 15$
$LaAl_3$	-0.44	$14 \times 14 \times 15$
$LaAlO_3$	-3.71	$4 \times 4 \times 2$
Li_2Al	-0.16	$15 \times 15 \times 15$
Li_3Al_2	-0.18	$16 \times 16 \times 16$
Li_5AlO_4	-2.5	$3 \times 3 \times 3$
LiAl	-0.17	$16 \times 16 \times 16$
$LiAl_3$	-0.09	$15 \times 15 \times 15$
$LiAl_5O_8$	-3.39	$3 \times 3 \times 3$
$LiAlO_2$	-3.07	$4 \times 4 \times 4$
Zr_2Al_3	-0.52	$15 \times 15 \times 15$
Zr_3Al	-0.32	$15 \times 15 \times 15$
Zr_4Al_3	-0.47	$15 \times 15 \times 14$
$ZrAl_2$	-0.55	$15 \times 15 \times 13$
$ZrAl_3$	-0.5	$16 \times 16 \times 18$

Table S5: Energy of formation per atom and **k** points for competing phases including Ga calculated using the PBEsol functional.

Phases	Energy/atom (eV)	**k** points (Γ-centred)
Ga_2O_3	-2.32	$7 \times 7 \times 4$
$La_3Ga_5O_{12}$	-2.95	$3 \times 3 \times 3$
$La_4Ga_2O_9$	-3.38	$3 \times 2 \times 2$
La_5Ga_3	-0.46	$13 \times 13 \times 12$
LaGa	-0.58	$15 \times 15 \times 15$
$LaGa_2$	-0.71	$16 \times 16 \times 15$
$LaGa_6$	-0.4	$14 \times 14 \times 13$
Li_2Ga	-0.3	$15 \times 15 \times 15$
Li_2Ga_7	-0.18	$13 \times 13 \times 13$
Li_5Ga_4	-0.34	$16 \times 16 \times 13$
Li_5GaO_4	-2.22	$3 \times 3 \times 3$
LiGa	-0.33	$16 \times 16 \times 16$
$LiGa_5O_8$	-2.38	$3 \times 3 \times 3$
$LiGaO_2$	-2.37	$4 \times 4 \times 4$
Zr_2Ga	-0.49	$15 \times 15 \times 15$
Zr_2Ga_3	-0.67	$15 \times 15 \times 15$
Zr_3Ga_2	-0.58	$13 \times 13 \times 16$
Zr_3Ga_5	-0.66	$14 \times 14 \times 13$
ZrGa	-0.67	$16 \times 16 \times 18$
$ZrGa_2$	-0.63	$16 \times 16 \times 15$
$ZrGa_3$	-0.56	$16 \times 16 \times 18$

Table S6: Energy of formation per atom and **k** points for competing phases including Nb calculated using the PBEsol functional.

Phases	Energy/atom (eV)	**k** points (Γ-centred)
La_3NbO_7	-3.77	$3 \times 3 \times 2$
$LaNb_7O_{12}$	-3.01	$2 \times 3 \times 2$
$LaNbO_4$	-3.63	$5 \times 5 \times 6$
Li_3NbO_4	-2.8	$4 \times 4 \times 4$
$Li_8Nb_2O_9$	-2.7	$4 \times 3 \times 2$
$LiNb_3O_8$	-3.11	$3 \times 4 \times 2$
$LiNbO_2$	-2.81	$8 \times 8 \times 2$
$LiNbO_3$	-3.01	$5 \times 5 \times 5$
Nb_2O_5	-3.16	$2 \times 6 \times 2$
NbO	-2.44	$5 \times 5 \times 5$
NbO_2	-3.05	$4 \times 4 \times 3$

Table S7: Energy of formation per atom and **k** points for competing phases including Ta calculated using the PBEsol functional.

Phases	Energy/atom (eV)	**k** points (Γ-centred)
La_3TaO_7	-3.82	$4 \times 4 \times 3$
$LaTa_3O_9$	-3.5	$4 \times 4 \times 3$
$LaTa_7O_{19}$	-3.43	$4 \times 4 \times 1$
$LaTaO_4$	-3.7	$3 \times 4 \times 3$
$LaZrTa_3O_{11}$	-3.6	$4 \times 4 \times 2$
Li_3TaO_4	-2.86	$4 \times 4 \times 3$
Li_5TaO_5	-2.66	$6 \times 6 \times 4$
$LiTa_3O_8$	-3.23	$3 \times 3 \times 4$
$LiTaO_3$	-3.12	$5 \times 5 \times 5$
Ta_2O_5	-3.28	$6 \times 6 \times 2$

Table S8: Energy of formation per atom and **k** points for competing phases including Y calculated using the PBEsol functional.

Phases	Energy/atom (eV)	**k** points (Γ-centred)
$LiYO_2$	-3.31	$4 \times 4 \times 4$
Y_2O_3	-4.04	$3 \times 3 \times 3$
$Y_4Zr_3O_{12}$	-4.02	$4 \times 4 \times 4$

Table S9 displays energies of formation for the limiting phases from the PBEsol calculations, calculated using the HSE06 functional.

Table S9: Energy of formation per atom from DFT calculations with HSE06. The **k** points stated above is also used for these calculations.

LLZO-phases	Energy/atom	Al-phases	Energy/atom	Ga-phases	Energy/atom	Nb-phases	Energy/atom	Ta-phases	Energy/atom	Y-phases	Energy/atom
La_2O_3	-3.58 eV	Al_2O_3	-3.2 eV	Ga_2O_3	-2.0 eV	$Li_8Nb_2O_9$	-2.47 eV	La_3TaO_7	-3.52 eV	$LiYO_2$	-6.46 eV
$La_2Zr_2O_7$	-3.72 eV	$La_4Al_2O_9$	-3.54 eV	Li_5GaO_4	-2.03 eV			Li_3TaO_4	-2.59 eV	Y_2O_3	-3.8 eV
Li_2O	-1.92 eV	Li_5AlO_4	-2.33 eV	$LiGaO_2$	-2.13 eV			Li_5TaO_5	-2.43 eV		
Li_2O_2	-1.47 eV	$LiAlO_2$	-2.88 eV	ZrGa	-0.74 eV			Ta_2O_5	-2.91 eV		
Li_2ZrO_3	-2.89 eV	Zr_3Al	-0.3 eV	$ZrGa_2$	-0.66 eV						
$Li_6Zr_2O_7$	-2.72 eV	Zr_4Al_3	-0.53 eV								
LiO_8	0.11 eV										
Zr_3O	-1.49 eV										
ZrO_2	-3.66 eV										

Figure S4 shows results from our initial screening of thermodynamic transition levels for intrinsic point defects in tetragonal LLZO using the PBEsol functional.

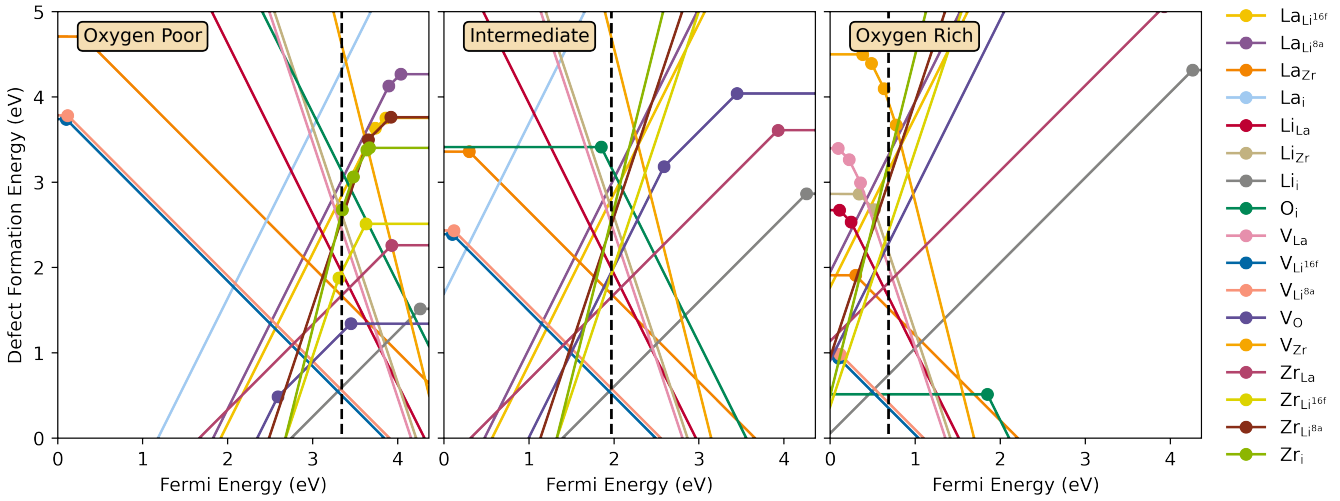

Figure S4: Transition level diagrams for the formation energies of intrinsic defects calculated using the PBEsol functional. In each panel the Fermi energy ranges from the valence band maximum (VBM) at 0eV to the conduction band minimum (CBM) at ~ 4.3 eV. The black dashed vertical lines display the self-consistent Fermi level.

Calculated thermodynamic transition levels for both pristine and doped LLZO at oxygen poor and oxygen rich sintering conditions are displayed in Figure S5 and S6, respectively.

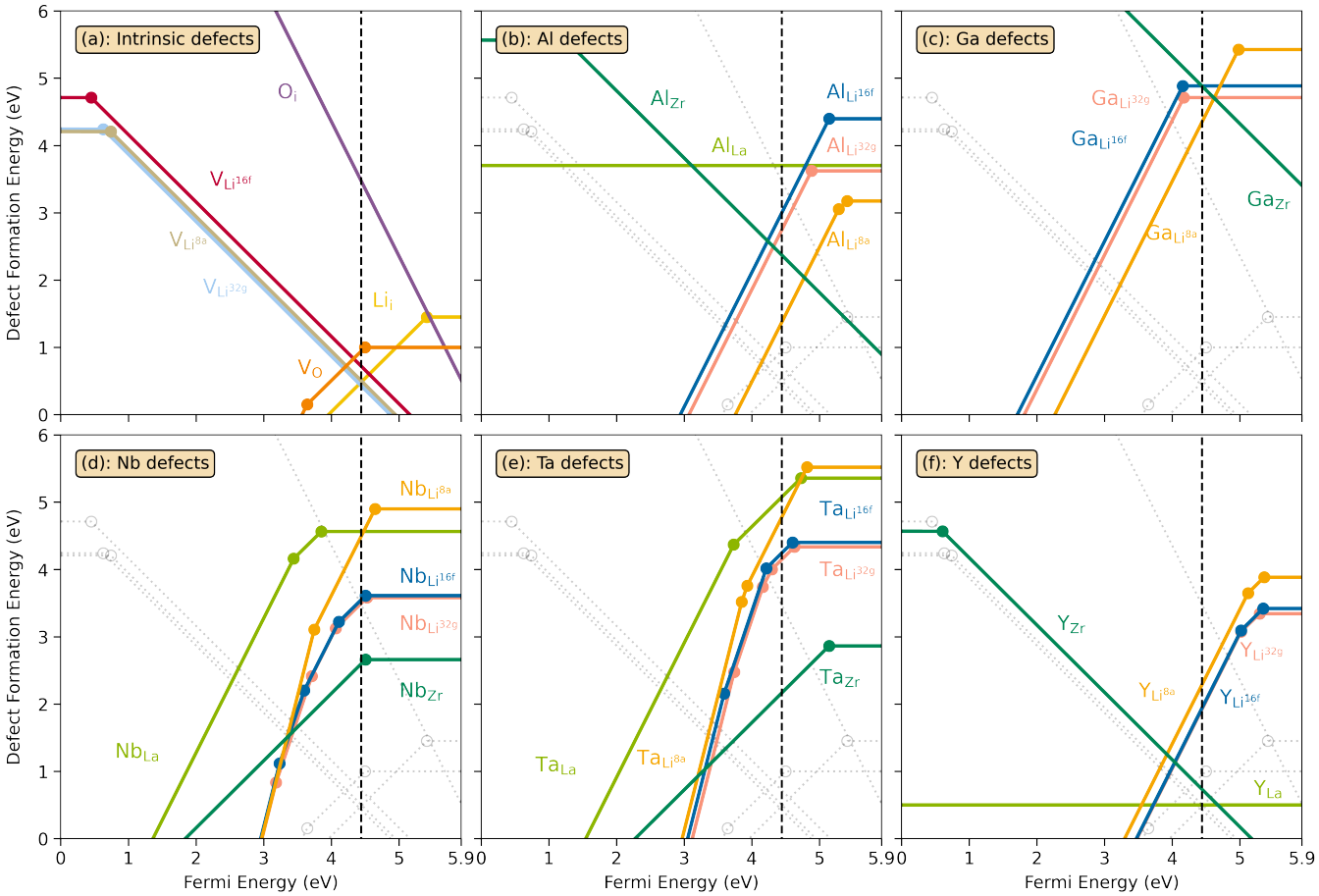

Figure S5: Transition level diagrams for the formation energies of intrinsic defects (a) and selected dopants: Al (b), Ga (c), Nb (d), Ta (e) and Y (f). In each panel, the Fermi energy ranges from the valence band maximum (VBM) at 0 eV to the conduction band minimum (CBM) at $\sim$ 5.9 eV. The chemical potentials, used for the calculated formation energies, were chosen to resemble sintering in an oxygen poor environment at 1200 °C and are displayed in SI figure S2. The black dashed vertical lines display the self-consistent Fermi level. Intrinsic defects are also displayed together with dopants as grey, transparent lines for clarity.

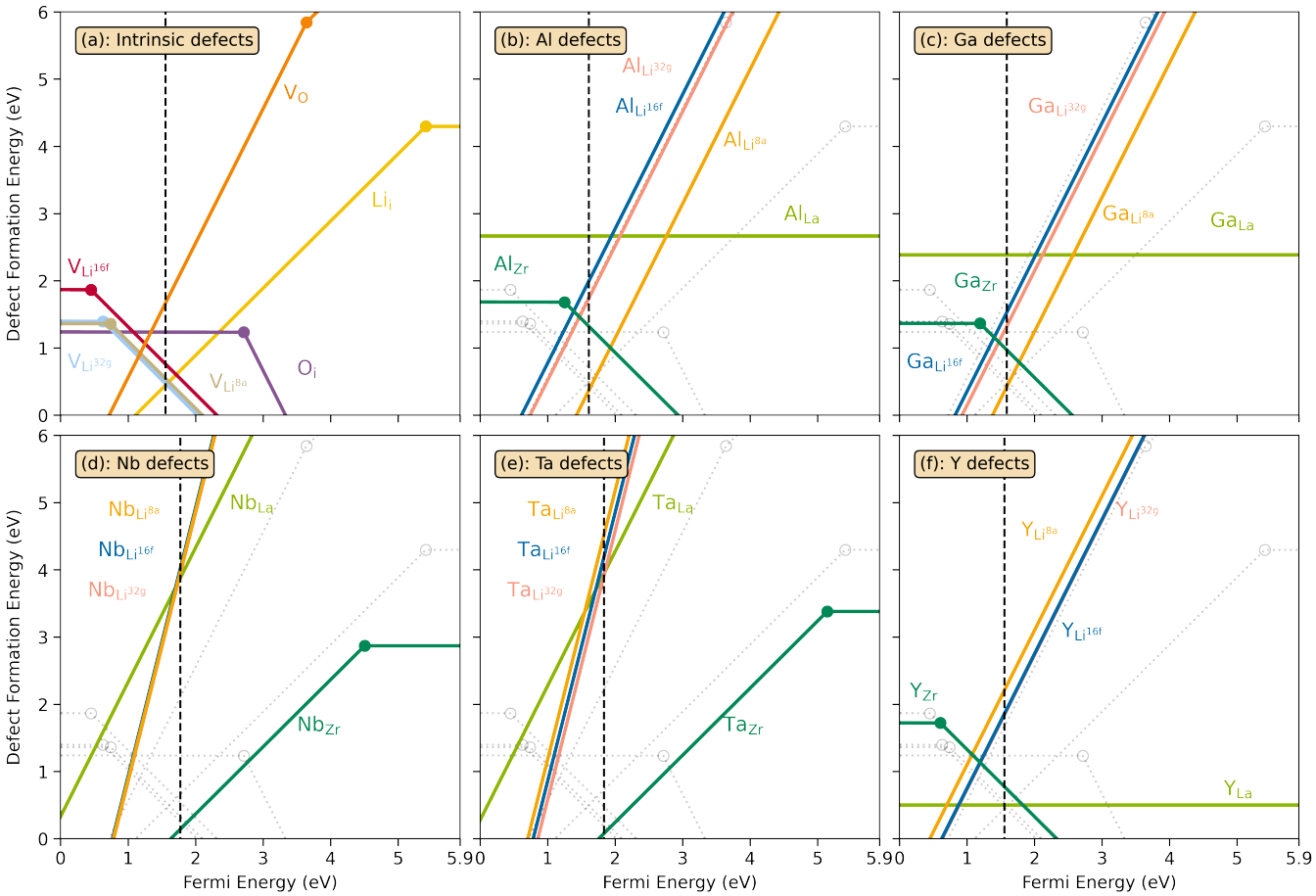

Figure S6: Transition level diagrams for the formation energies of intrinsic defects (a) and selected dopants: Al (b), Ga (c), Nb (d), Ta (e) and Y (f). In each panel, the Fermi energy ranges from the valence band maximum (VBM) at 0 eV to the conduction band minimum (CBM) at $\sim$ 5.9 eV. The chemical potentials, used for the calculated formation energies, were chosen to resemble sintering in an oxygen rich environment at 1200 °C and are displayed in SI figure S2. The black dashed vertical lines display the self-consistent Fermi level. Intrinsic defects are also displayed together with dopants as grey, transparent lines for clarity.

Transition levels from charged to neutral states are listed in Table S10 for all defects resulting from the dopants investigated. All defects are either deep donors or deep acceptors.

Table S10: Transition levels for defects transitioning to the neutral charged state given as eV above the valence band maximum (VBM).

	Li_{8a}	Li_{16f}	Li_{32g}	La	Zr
Al	5.41	5.14	4.88	-	1.25
Ga	4.98	4.16	4.17	-	1.19
Nb	4.65	4.50	4.53	3.85	4.50
Ta	4.82	4.60	4.63	4.73	5.14
Y	5.36	5.34	5.29	-	0.61

A calculated orbital resolved electronic density of states (DOS) of pristine tetragonal LLZO is displayed in Figure S7. The VBM is set to 0 eV. The valence band is dominated by O_p, while the conduction band show mixing of La_d, La_f, O_p, and Zr_d.

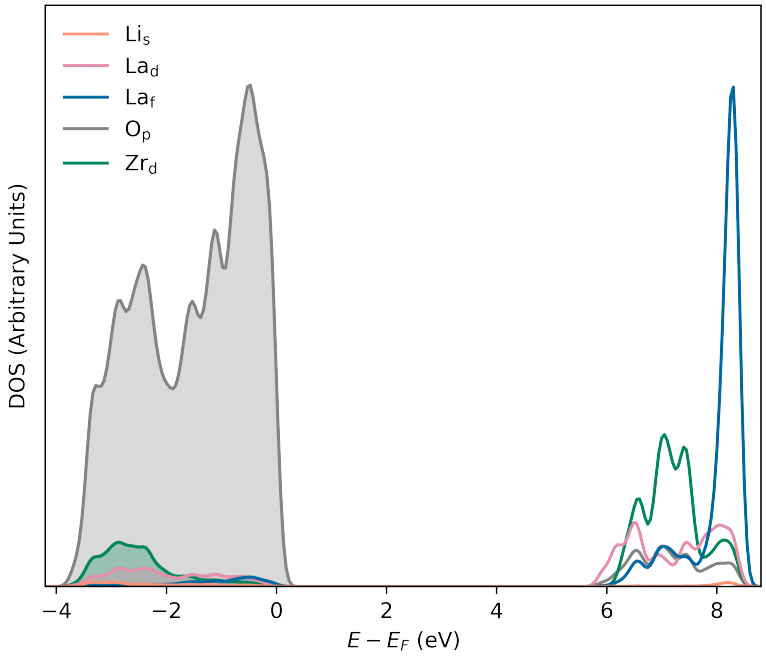

Figure S7: Orbital resolved density of states calculated using the HSE06 functional.

[1] Aliaksandr V. Krukau, Oleg A. Vydrov, Artur F. Izmaylov, and Gustavo E. Scuseria. Influence of the exchange screening parameter on the performance of screened hybrid functionals. *The Journal of Chemical Physics*, 125(22):224106, 2006.

[2] Koichi Momma and Fujio Izumi. *VESTA3* for three-dimensional visualization of crystal, volumetric and morphology data. *Journal of Applied Crystallography*, 44(6):1272–1276, Dec 2011.

[3] John P. Perdew, Adrienn Ruzsinszky, Gábor I. Csonka, Oleg A. Vydrov, Gustavo E. Scuseria, Lucian A. Constantin, Xiaolan Zhou, and Kieron Burke. Restoring the Density-Gradient Expansion for Exchange in Solids and Surfaces. *Phys. Rev. Lett.*, 100:136406, Apr 2008.